

Comparative Study of 3-Bladed and Scissors Tail Rotors Aerodynamics in Axial Flow

Pavel V. Makeev¹, Yuri M. Ignatkin¹, Alexander I. Shomov¹, Valery A. Ivchin²

Abstract – The paper is focused on the numerical study of the aerodynamic characteristics of 3-bladed and scissors tail rotors used on Mi-8/17 series helicopters. The hovering and axial flow modes, including the Vortex Ring State (VRS) area are considered. The free wake model developed by authors is used in the research. The study has been performed for two approaches: with a fixed blade pitch angle and with a fixed time-average thrust value. The dependences of the rotor thrust and torque coefficients vs. axial flow velocity and vs. number of revolutions of a rotor have been obtained. The vortex wake shapes and flow images via streamlines have been analyzed. The comparative analysis of the results has been performed. Scissors rotor demonstrates better aerodynamic characteristics in comparison with 3-bladed rotor. Among them: increased hovering efficiency, lower level of thrust and torque pulsations in the VRS modes, smaller power consumption while constant thrust. The authors came to the conclusion about the greater efficiency of the aerodynamic design of scissors tail rotor compared to 3-bladed rotor both in hover and in the VRS modes area. **Copyright © 2022 The Authors.**

Published by Praise Worthy Prize S.r.l. This article is open access published under the CC BY-NC-ND license (<http://creativecommons.org/licenses/by-nc-nd/3.0/>).

Keywords: Tail Rotor, Free Wake Model, Hover, Vortex Ring State, Aerodynamic Performance

Nomenclature

| | |
|---------------|--|
| ρ | Air density [kg/m ³] |
| t | Time [s] |
| R | Rotor radius [m] |
| α_R | Angle of attack of a rotor [degree] |
| β | Angle of slip [degree] |
| N_b | Number of blades |
| c | Blade chord [m] |
| σ | Rotor solidity, $N_b c / \pi R$ |
| θ_{tw} | Blade twist, degree |
| θ | Blade pitch angle [degree] |
| ωR | Rotor blade tip speed [m/s] |
| n | Number of revolutions of a rotor |
| V_y | Axial flow velocity [m/s] |
| T | Rotor thrust [N] |
| Q | Rotor torque (N m) |
| c_T | Rotor thrust coefficient $(2T)/(\rho(\omega R)^2 \pi R^2)$ |
| c_Q | Rotor torque coefficient $(2Q)/(\rho(\omega R)^2 \pi R^3)$ |
| c_{Qh} | Rotor torque coefficient in hover |
| VRS | Vortex Ring State |
| UCB | Upper Couple of Blades |
| LCB | Lower Couple of Blades |

I. Introduction

Axial flow modes (when direction of free stream coincides with rotor axis) belong to the main operational modes of helicopter rotor. They include hovering modes and flowing with positive/negative angle of attack of

rotor, when free stream direction matches/doesn't match with rotor's thrust direction. Among the modes of flowing with a positive angle of attack, the Vortex Ring State (VRS) modes observed in a certain speed range are particularly distinguished. They are characterized by a number of features related to the rotor's aerodynamics such as: decrease in the rotor thrust, increase in the power consumptions, rotor thrust and torque pulsations, unstable rotor flowing. Since the 1950s, some experimental and computational studies have been dedicated to aerodynamics of the rotor in the VRS modes. The experimental study of the VRS modes is a technically complex problem also associated with large material costs. This is especially true for studies of full-scale rotors and large-scale models of rotors. The existing experiments have used the rotors with different geometries and sizes from full-scale to small-scale. For experimental investigations of the VRS modes various Wind Tunnels (WT) as well as other special experimental stands are using. The work by Drees & Hendl [1] have used WT and widely known due to the first clearly results of smoke visualization of the flow structure around the rotor in the VRS mode. The work by Castle and Gray [2], dedicated to WT (with 2.7-m diameter) testing of four models of rotors (with diameter of 1.2-m and 1.8-m) under various axial flow modes, including the VRS modes. Yaggy & Mort [3] are focused on the study of 3 m and 3.6 m full-scale propellers in WT with 2.1×3-working section. The work by Washizu et al. [4] is performed using special experimental stand consisting of

a model rotor with a diameter of 1.1-m mounted on a movable trolley mounted on a movable trolley. The work by Empey & Ormiston [5] has been carried out for the main and tail rotor models of the AH-1G helicopter on the 1/8 scale also in the WT. In the work by Xin & Gao [6] the aerodynamic characteristics of the model rotor are studied using the original rotary stand where a model of a two-bladed rotor with a diameter of 1.1-m has been installed at the end of a rotating beam. Brinson & Ellenrieder [7] have tested the model of a rotor with diameter of 1.54-m using 2.6×5.5-m WT. In the work by Betzina [8] model of tiltrotor (1.2 m diameter) have been tested in WT with working section of 24×36-m.

Caradonna [10] has tested 2-bladed rotor in WT with 2.1×3-m working section. In the work by Green et al. [9] the study of the three-bladed small scale model rotor (with blade radius of 0.075-m) in WT with 1.5×0.85-m working section has been carried out. The work by Stack et al. [11] use water tunnel and small-scale rotor with diameter of 0.25 m. Efimov & Chernigin [12] have investigated small-scale 2-bladed propeller in WT with 0.4×0.6-m working section. With the development of computer technology, various methods of Computational Fluid Dynamics (CFD) have been used to study the VRS modes. Nowadays mathematical modeling approaches based on vortex models are widely used. For example, in the work by Leishman et al. [13] a single rotor, tandem rotor and tiltrotor are considered with the original free-vortex wake model. In the work by Celi & Ribera [14] a simulation of the vertical descent of a single main rotor helicopter with passing through the VRS-area has been performed. Bailly [18] have used two various numerical models developed by Eurocopter and ONERA and modelled the Dauphin helicopter in the VRS modes using flight test data. Work by Krinsky & Sheglova [19] is based on a free vortex wake model developed at TsAGI (Russia). In recent years, the finite volume method (FVM) has also become common for modeling the VRS modes of a rotor. As a rule, an approach based on the solution of the Unsteady Reynolds Averaged Navier-Stokes equations (URANS) with the use of various turbulence models is used. The work by Stalewski & Surmacz [17] use the URANS method with the Virtual Blade Model to conduct the helicopter flight simulations, in a vicinity of the VRS boundaries. Mohd & Barakos [18] use the URANS method to study the VRS modes of the two-blade rotor. The work by Kinzel et al. [19] contains the results of URANS studies of the coaxial rotor at vertical descent, including "vortex ring" modes. It considers a models of the coaxial and conventional four-bladed rotors of the Unmanned Aerial Vehicle (UAV). McQuaid et al. [20] have also investigated the VRS modes using URANS method.

Their work is dedicated to development of VRS prediction system for small-scale quadrotor UAV. The works of Ryan et al. [21] and Dong & Vire [22] have been focused not on the study of VRS modes of aerial vehicle rotors, but on the VRS modes of offshore wind turbines rotors. It should be noted that the analysis of the

results of studies of the VRS modes shows their significant dependence on both the geometric and kinematic parameters of the rotors, and on the test conditions. This indicates the need to conduct a study of rotors in full-scale conditions, which is achievable today with the help of numerical modeling. The study of the axial flow modes is important not only for the main rotor, but also for the tail rotor. The tail rotor provides directional control of the helicopter and the loss of its effectiveness due to falling into the VRS modes, for example, in a crosswind flight, can lead to a flight accident. Thus, study of the aerodynamic characteristics of the tail rotor in axial flow modes including in the VRS modes is an actual task of helicopter aerodynamics.

The original free wake model used in the presented work has been developed at Moscow Aviation Institute [23] by the authors. Previously, this model has been applied in study of the aerodynamic characteristics of conventional [24] and coaxial [25] rotors in the hover state and VRS modes. In these works, the model has been validated by comparing the results of calculations with experimental and calculated data of the other authors.

The presented work is dedicated to a numerical study of the aerodynamic characteristics of two types of tail rotors used on Mi-8/17 helicopter series. This is a 3-bladed tail rotor used on Mi-8 helicopters and a 4-bladed scissors tail rotor, used on new versions of Mi-17 helicopters. The first part of the study examines the hovering modes. The second part is dedicated to the axial flow modes. Special attention has been paid to the axial flow modes with a positive angle of attack including the VRS modes area. For the tail rotor that is equal to flight with a crosswind coincide with the tail rotor's thrust direction. The presented work focused on the comparative analysis of the obtained aerodynamic characteristics.

II. Method and Object of Study

II.1. Free Wake Model of a Rotor

The free wake model of the rotor developed at the Helicopter Design Department of Moscow Aviation Institute is based on the lifting line theory and the blade element theory. Each blade element is modeled by an attached vortex segment located on a quarter of the blade element chord c (Fig. 1) with the control point in the center of the segment. For each time step Δt a quadrangular contour consisting of vortex segments with a constant circulation Γ (equal to the attached vortex circulation) descends from the blade element. The circulation of the attached vortex changes along the blade radius and depends on the blade azimuthal position.

Determining of the attached vortex circulation is implemented through an iterative method. The coefficients of the lift force c_L and the drag force c_D of the blade element are determined at the found angle of attack α and the total flow velocity W based on airfoil steady test data in wind tunnel. The system of vortex

contours creates a free vortex wake in the form of a grid of longitudinal and transverse vortex segments (Fig. 1).

The vortex wake grid is deformed at each calculated step under the influence of external and induced velocity fields. A key part of the model is calculation of induced velocities from the vortex segment which is an element of the free vortex wake grid. Here it is used an approach that allows determining the vorticity field from the vortex segment and the induced velocity from this vorticity field on the basis of an exact solution of the vortex source diffusion. The model with its basic equations is described in detail in works [23], [25].

II.2. Computational Models of the Tail Rotors

The main characteristics of the scissors and 3-bladed tail rotors under study are shown in Table I. Figures 2 show the geometry of computational models of scissors and 3-bladed tail rotors. The rotor blades have been modeled as absolutely rigid and each of them consisted of 12 calculated elements. The scissors rotor consists of two two-bladed rotors (Upper (UCB) and Lower (LCB) Couples of Blades), with the planes of rotation spaced by the value h . The UCB and LCB are installed with the angle of the scissors χ (Fig. 2(b)). The considered scissors rotor has a L-configuration with LCB advancing blade. The model has covered the flapping movement of the blades: relative to gimbal in the case of 3-bladed rotor and relative to combined horizontal hinges for scissors rotor. The calculated time step in both cases was $\Delta t = 0.00148$ seconds, which corresponds to the azimuthal angle $\Delta\psi = 10^\circ$. The total number of revolutions of the rotor for each calculation was $n = 160$ or 5760 calculated time steps (approximately 8.5 seconds in real time).

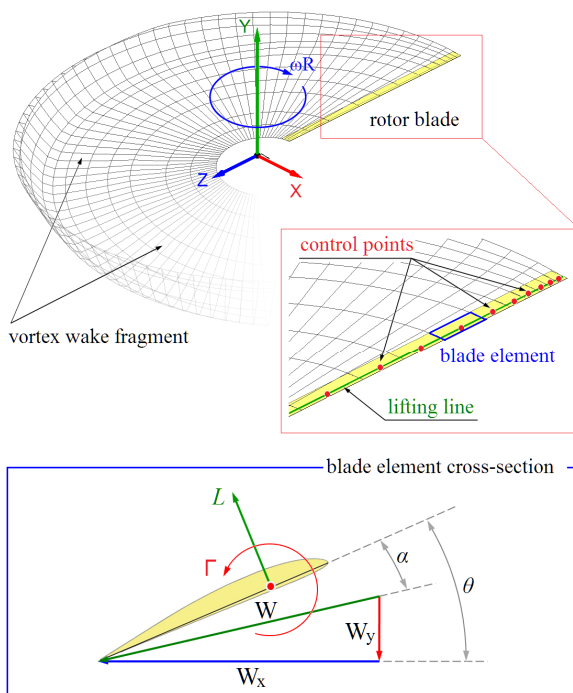
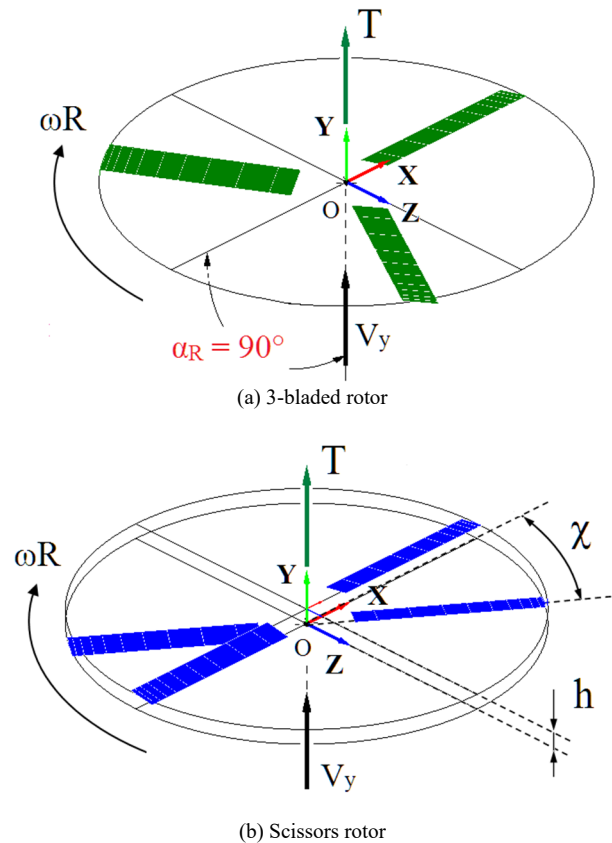


Fig. 1. Free wake model

TABLE I
PARAMETERS OF THE ROTORS UNDER STUDY

| Tail rotor type | 3-bladed | Scissors |
|-------------------------------------|-------------|-------------|
| Rotor diameter, D [m] | 3.9 | 3.84 |
| Number of blades, N_b | 3 | 4 |
| Blade chord, c [m] | 0.305 | 0.24 |
| Rotor solidity, σ | 0.149 | 0.159 |
| UCB/LCB distance, h [m] | - | 0,135 |
| "scissors" angle, χ [degree] | - | 36 |
| Blade tip speed, ωR [m/s] | 230 | 230 |
| Blade airfoil | NACA 230M | TsAGI |
| Blade twist, θ_{tw} [degree] | 0 | 0 |
| Blade shape | rectangular | rectangular |



Figs. 2. Scheme of rotors under study

The pitch angles of the upper and lower pairs of blades of the scissors rotor were the same in the calculations: $\theta_U = \theta_L$. The axial flow modes are calculated in the flow velocity range of $V_y = -15 - 25$ m/s in step of 3 – 5 m/s for negative angles of attack of the rotor ($\alpha_R = -90^\circ$, $V_y = -15 - 0$ m/s) and in step of 1 – 2 m/s for positive angles of attack of the rotor ($\alpha_R = 90^\circ$, $V_y = 0 - 25$ m/s).

III. Results and Discussion

III.1. Hovering Modes

There is a number of works dedicated to the analysis of the scissors (stacked) rotor aerodynamics in hovering modes and the determination of its optimal geometry [26]-[32]. It is known that the advantages of the scissors rotor are associated with its improved aerodynamic

design. A distinctive feature of the scissors rotor is the separation of the rotation planes of the upper and lower couple of blades, as well as the presence of a "scissors" angle (Figs. 2). The scissors rotor considered in presented study has a L-configuration, which is the most optimal from the point of view of the maximum figure of merit values [26]. In addition, the scissors rotor has 4 blades compared to 3 for a 3-bladed rotor and a more perfect aerodynamic airfoil of the blade. Below there are the results of the comparative analysis of the aerodynamic characteristics of the 3-blade and scissors rotors of the Mi-8/17 helicopter series in hovering modes. Figures 3 and 4 show rotor performance diagrams and diagrams of Figure of Merit vs. rotor blade pitch angles in hover. In Fig. 3 for the 3-bladed rotor, the data of an experiment conducted at the JSC Mil & Kamov are also presented. It is clear that the calculated results are in good agreement with experimental data. From performance diagrams on Fig. 3 it follows that with the same thrust coefficients c_T the scissors rotor has smaller values of torque coefficients c_Q than 3-bladed rotor. This is reflected in the FoM ratio diagrams shown in Fig. 4.

The FoM values of scissors rotor are 10% higher than FoM values of 3-bladed rotor. The advantages of scissors rotor are due to its improved aerodynamic design [26]-[28]. It includes: 1) a larger number of blades in scissors rotor (4 vs. 3 for 3-bladed rotor); 2) a positive effect of interference between the upper and lower couple of blades, provided by separation of rotational planes and by angle of the "scissors" χ (Figures 2, 3) usage of the advanced aerodynamic airfoil.

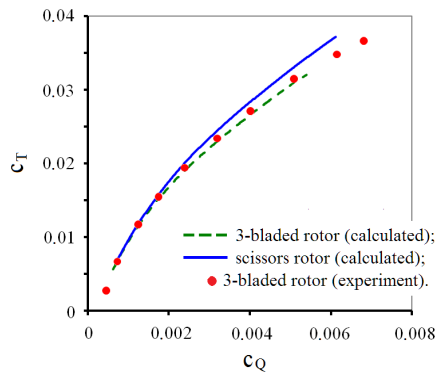


Fig. 3. Calculated and experimental performance diagrams

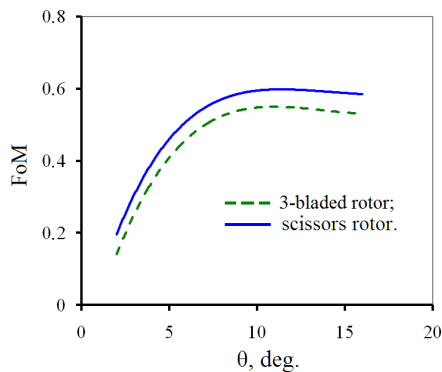


Fig. 4. Figure of Merit diagrams

Figures 5 show the visualization of the vortex wake shapes of 3-bladed (Fig. 5(a)) and scissors (Fig. 5(b)) rotor in the hover ($c_T = 0.02 = \text{const}$).

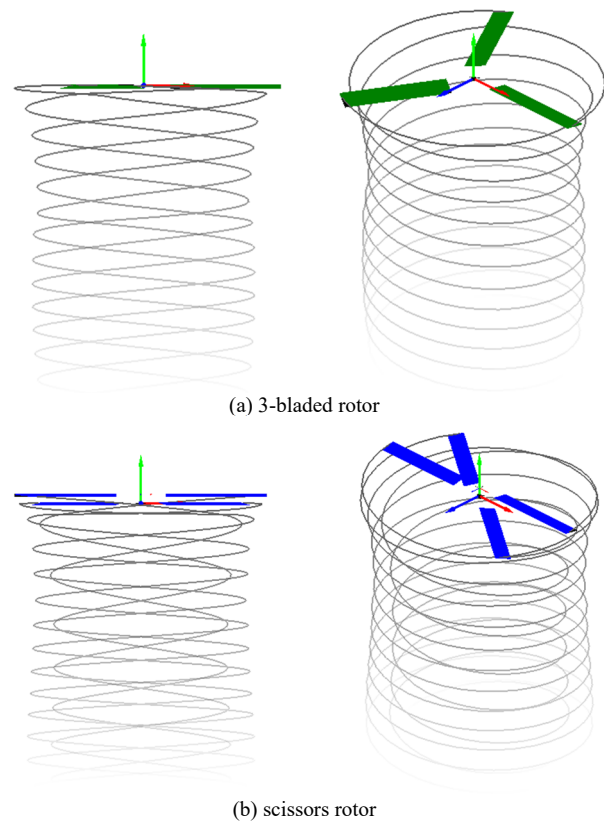
Here are presented only the blade tip vortices. In both cases, there is a characteristic compression of the vortex wake behind the rotors, which is typical for hovering modes.

From Fig. 5(b) it can be seen that blade tip vortices of upper couple of blades have a greater compression and move downwards at much higher speeds than lower couple of blades. This fact is caused by the distance between the rotational planes of upper and lower couple of blades of scissors rotor [29]-[32] and is also observed in coaxial counter-rotating rotors [33], [34]. Figures 6 show visualization of flow structure around a rotor. Pictures of flow on Figs. 6 are built in OXY plane using streamlines.

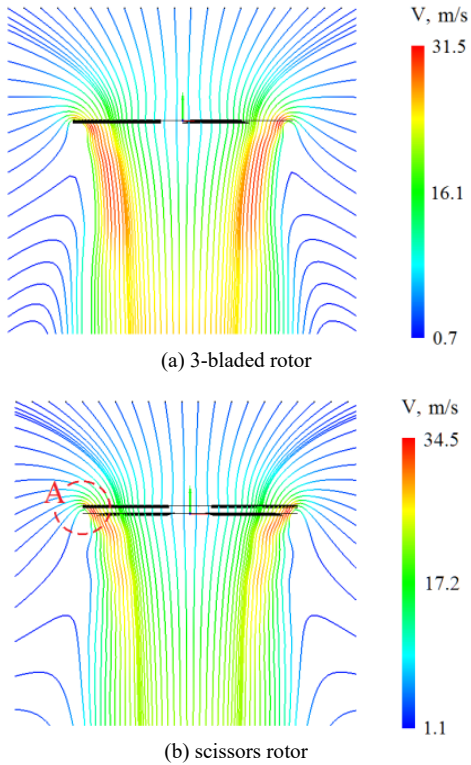
There is also observed compression of jet behind the rotor.

In case of scissors rotor, due to the separation of the rotation planes of the upper and lower couple of blades ($h/R \approx 0.07$), an additional air flow passes through the rotation plane of the lower couple of blades. In this case, the total area through which the flow passes increases. This feature is highlighted by zone "A" in Fig. 6(b).

Thus, the feature of coaxial rotors, which usually have a rotational plane spacing of $0.2R$ [33], is partially realized in considered scissors rotor. This improves the aerodynamic performance of the scissors rotor compared to a 3-bladed rotor with a single plane of blades.



Figs. 5. Wake shapes in hover



Figs. 6. Visualization of flow around a rotors using streamlines

For the equal blade pitch angles ($\theta_U = \theta_L$) the upper and lower couple of blades of the scissors rotor have different performance due to aerodynamic interference [29]. Figure 7 and Figure 8 show diagrams of thrust and torque coefficients distribution between the couple of blades, depending on the pitch angle θ . It can be seen that for scissors rotor, the lower couple of blades has a greater thrust and less torque than the upper couple.

III.2. Axial Flow Modes

The axial flow modes include the modes when the rotor operates with a negative angle of attack $\alpha_R = -90^\circ$ and a positive angle of attack $\alpha_R = 90^\circ$ (Figs. 2). The positive angle of attack is the most difficult to study.

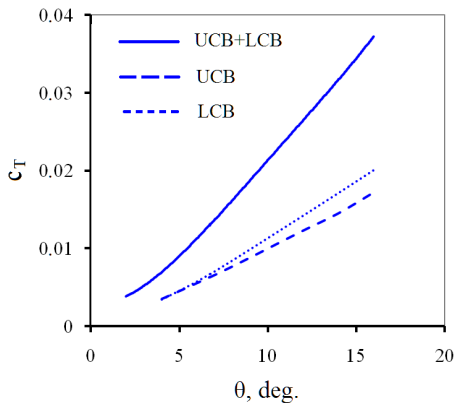


Fig. 7. The distribution of thrust between the UCB and LCB of the scissors rotor ($\theta_U = \theta_L$)

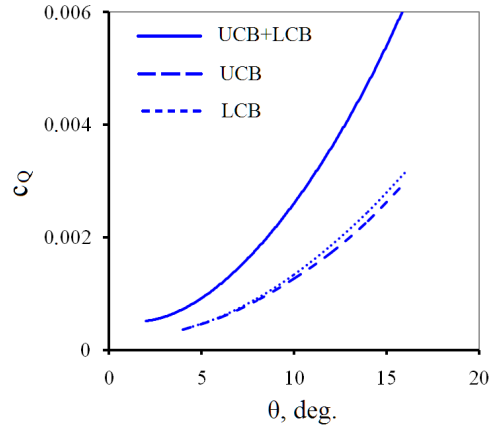


Fig. 8. The distribution of torque between the UCB and LCB of the scissors rotor ($\theta_U = \theta_L$)

There is a certain range of incoming flow velocities when the rotor enters the operating modes known as Vortex Ring State (VRS) modes. One of the criteria of the rotor falling into the VRS modes is a decrease of rotor thrust at the fixed blade pitch angle $\theta = \text{const}$. This approach to investigation of VRS modes is used in both experimental [2]-[6] and numerical [13], (16), [18] studies. In this case the borders of the VRS modes area are determined by reduction of the rotor thrust in comparison with the thrust in the hover. The results of investigations of 3-bladed and scissors rotor aerodynamic performance in axial flow modes in the range of $V_y = -15 - 25$ m/s are presented below. Calculations for each of the rotors have been made for a fixed blade pitch angles $\theta = \text{const}$ which provided the equal thrust coefficient in the hover $c_T = 0.02$ for both 3-bladed and scissors rotors.

Figure 9 shows the dependence of time-averaged thrust coefficients on axial flow velocity V_y . The values of the thrust coefficients c_T shown in Fig. 9 for each mode of operation of the rotor are average over time for the range of revolutions number $n = 20 - 160$. Thus, possible unsteady pulsations of the rotors thrust in time are not shown here. The thrust coefficient curves $c_T = f(V_y)$ obtained for both rotors are almost identical. A decrease of the rotor thrust relative to the hovering mode is observed for negative angle of attack $\alpha_R = -90^\circ$ and in the range of $V_y \approx 8.5 - 15.7$ m/s for $\alpha_R = -90^\circ$. At $V_y = 11 - 12$ m/s, the rotor's thrust is reduced to 79% of the hovering value. Therefore, at $V_y = 11 - 12$ m/s, both rotors reach the most critical "peak" VRS modes.

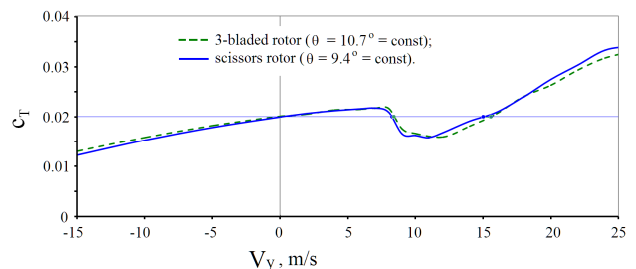


Fig. 9. Dependences of time-averaged thrust coefficient vs. axial flow velocity ($\theta = \text{const}$)

Figure 10 shows the curves of the rotor time-averaged torque coefficients c_Q . Scissors rotor has on average 10% lower values of torque coefficient c_Q than 3-bladed rotor for the equal rotor thrust values (Fig. 9). This means that with the same thrust, the scissors rotor will consume less power over the entire range of axial flow modes. From the results shown in Figs. 9 and 10, in particular, it follows that maintaining a constant thrust values in the area of VRS modes requires a significant increase in the power spent on rotation of the rotor. The increase in the required rotor power (rotor torque coefficient) at constant rotor thrust in comparison with the hovering mode is also one of the distinctive features of the VRS modes. At the same time, for each rate of free stream velocity V_y it is necessary to select the appropriate rotor blade pitch angles θ . This fact makes it difficult to conduct experimental studies. Numerical modeling in this approach also requires significant time and computational resources. For the considered 3-bladed and scissors rotors, the calculation of axial flow modes has been implemented in the free stream velocity range $V_y = -15 - 25$ m/s with a fixed time-averaged thrust coefficient $c_T = 0.02 = \text{const}$. Maintaining a constant time-averaged rotor thrust at different values of V_y has been ensured by selecting the relevant values of the rotor blade pitch angles θ . The results of these calculations are presented below. Figure 11 shows the dependences of the required rotor blade pitch angles on free stream velocity rate V_y . These rotor blade pitch angles have been used in the calculations and obtained from the requirement of providing the constant time-averaged rotor thrust values.

The areas (for $\alpha_R = 90^\circ$) where the required blade pitch angles exceed the values for the hovering modes can be used as boundaries of the VRS modes. Here, these values are $V_y \approx 7.5 - 16$ m/s for a 3-bladed rotor and $V_y \approx 7 - 14.6$ m/s for scissors rotor.

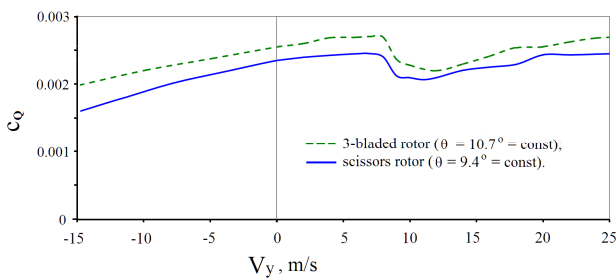


Fig. 10. Dependences of time-averaged torque coefficient vs. axial flow velocity ($\theta = \text{const}$)

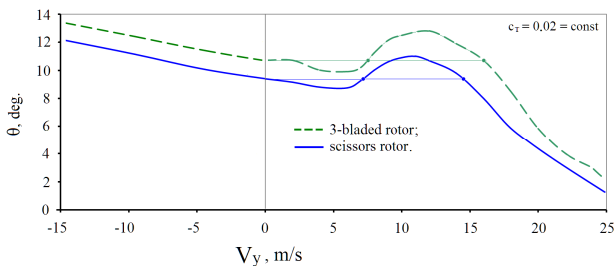


Fig. 11. Dependences of blade pitch angle values vs. axial flow velocity ($c_T = 0.02 = \text{const}$)

Figure 12 shows the dependences of time-averaged torque coefficient c_Q on free stream velocity rate V_y . Presented dependences have been obtained at constant rotor thrust values. For a 3-bladed rotor the region of $c_Q > c_{Qh}$ has been located within $V_y \approx 7.7 - 15$ m/s.

Meanwhile, at $V_y = 12$ m/s there is an increase in the rotor torque coefficient up to 126% of its value when hovering. At the same time for scissors rotor, $c_Q > c_{Qh}$ has been located within $V_y \approx 7.3 - 14$ m/s and the growth of c_Q at $V_y = 10$ m/s is up to 121% of the value in hover.

An important criterion for the analysis of the VRS modes is also the pulsation of rotor thrust and torque [4].

The amplitudes of rotor thrust $\Delta c_T = (c_{T\text{max}} - c_{T\text{min}})/2$ and torque $\Delta c_Q = (c_{Q\text{max}} - c_{Q\text{min}})/2$ pulsations obtained for the case of a constant time average thrust (Figs. 11 and 12) are shown in Figs. 13 and 14. Starting from the values of $V_y \approx 5 - 7$ m/s, pulsations of the thrust and torque coefficients are observed. According to the values of the amplitude of the thrust and torque pulsations (for example, 5%, 10%, 15%, etc.), the range of VRS modes is usually determined [4]. Figures 13 and 14 show that in the area of the VRS modes, the amplitudes of the rotor thrust and torque pulsations reach values up to 20 - 30% of the average values. Meanwhile, the scissors rotor at the most intense of VRS modes in the range of $V_y \approx 10 - 15$ m/s has a 1.5 - 2 times smaller amplitude of thrust and torque pulsations than the 3-bladed rotor. Even in early experimental studies [1], using smoke visualization, it was found that the structure of the flow around the rotor in the VRS modes is characterized by the formation of an "air body" with a circulating flow inside.

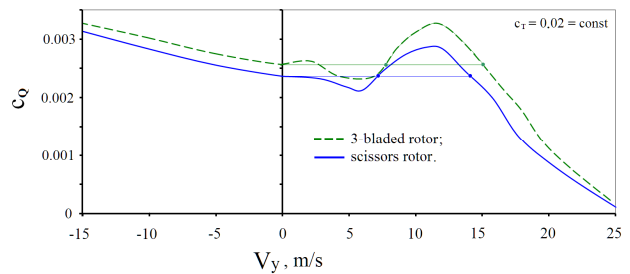


Fig. 12. Dependences of time-averaged torque coefficient values vs. axial flow velocity ($c_T = 0.02 = \text{const}$)

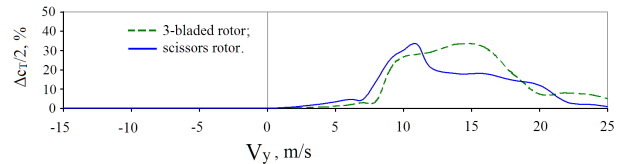


Fig. 13. Dependences of thrust coefficient pulsation amplitude vs. axial flow velocity ($c_T = 0.02 = \text{const}$)

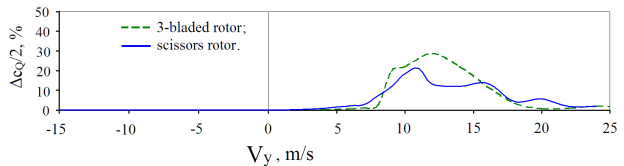


Fig. 14. Dependences of torque coefficient pulsation amplitude vs. axial flow velocity ($c_T = 0.02 = \text{const}$)

Figures 15 show the pictures of flow visualization for the 3-bladed and scissors rotors made using velocity fields and streamlines in the OXY plane for a fixed moment of time (for $c_T = 0.02 = \text{const}$). Flow pictures are shown for velocities $V_y = 10, 12, 14$ and 18 m/s belonging to the VRS modes area. The formation of a characteristic "air body" around the rotors is clearly visible. Depending on the incoming flow velocity V_y , the "air body" occupies a different position relative to the rotors rotational planes. At $V_y = 10$ m/s (Figs. 15(a) and 15(b)), the "air body" is shifted mainly downwards and is mostly located under the rotors. At $V_y = 12$ m/s (Figs. 15(c) and 15(d)), the "air body" shifts upwards and occupies an almost central position relative to the rotors rotational planes. This is related to the fact noted in the rotors performance analysis that the speed $V_y = 12$ m/s for both rotors corresponds to the "peak" VRS modes. In these modes, the values of the required blade pitch angles (Fig. 11) and the required torque coefficients c_Q (Fig. 12) are close to the maximum values. Also, attention is drawn to the fact that the dimensions of the "air body" of the X-shaped rotor are smaller than those of the 3-bladed rotor. With an increase in the V_y values, the "air body" begins to shift upward. For $V_y = 14$ m/s, such a displacement is observed for scissors rotor (Fig. 15(f)), but not observed yet for 3-bladed rotor (Fig. 15(e)). It was noted above, in Fig. 13, that at $V_y = 14$ m/s, the scissors rotor has almost twice less values of the thrust pulsations amplitude ($\Delta c_T/2 = 18\%$ versus 33% for a 3-bladed rotor). A similar thing is observed at $V_y = 14$ m/s for rotor torque (Fig. 14): for scissors rotor the amplitude of torque pulsations is $\Delta c_Q/2 = 12\%$ versus 22% for 3-bladed rotor. Figures 15(j) and 15(k) illustrate the flow pictures of the 3-bladed and scissors rotors for $V_y = 18$ m/s. It can be seen that the "air body" for both rotors at this V_y value is already significantly shifted upstream, so that its lower boundary comes close to the rotor rotational plane. At the same time, the amplitudes of thrust pulsations are reduced by 2 – 3 times compared to the "peak" modes of the VRS, and the amplitudes of the torque by 4 – 5 times. This indicates that the rotors at the value of $V_y = 18$ m/s begin to exit the VRS modes area.

Thus, Figures 15 show illustrations of the flow structures of the rotors for a number of the most typical velocities V_y entering the VRS modes area. The reason for the pulsations of rotor's thrust and torque in the VRS modes is the unsteady flow around. Over time, the "air body" shown in Figs. 15 for fixed moments of time (corresponding to the $c_T = 0.02 = \text{const}$) changes its shape and oscillates relative to the rotor's rotational plane with the change in the shape of rotor's vortex wake.

Figures 16 show the results of visualization of the vortex wake shapes for the 3-bladed (Fig. 16(a)) and scissors (Fig. 16(b)) rotors at $V_y = 12$ m/s. The wake shapes are presented for a number of fixed moments of time (the number of revolutions of the rotors $n = 60, 80, 100, 120, 140$) in two projections for the side and top views. It can be seen that the shapes of the vortex wake in the VRS modes for different flow velocities are

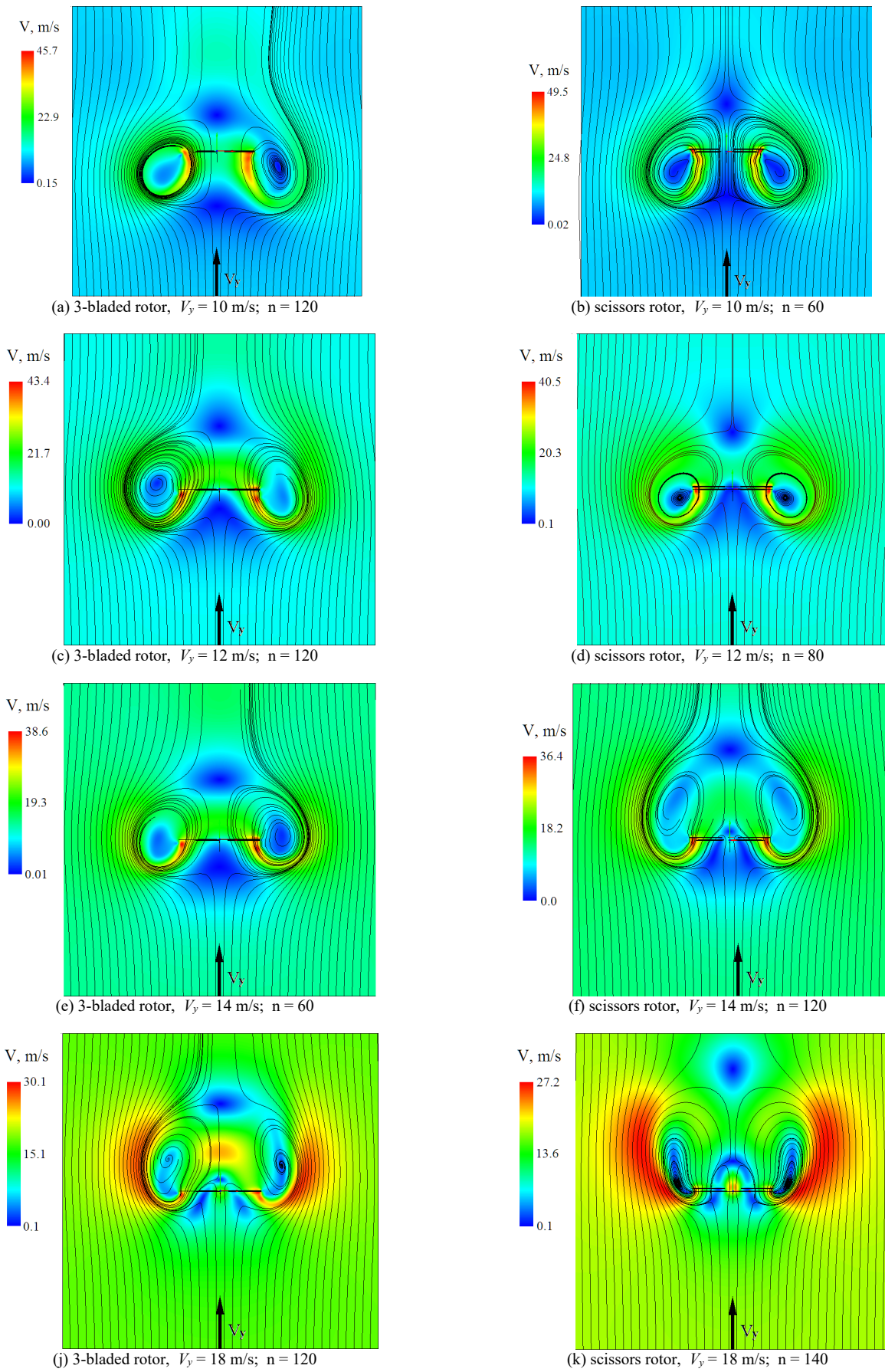
extremely complex and nonlinear. In addition, over time, the shape of the vortex wake has significant changes, which affects the current values of thrust and torque and causes their pulsations in time. Separately, we note the observed asymmetry of the vortex wake relative to the rotor's axis OY. Due to the indicated asymmetry the rotor blades rotate in an asymmetric induced velocities field, which also affects the instantaneous rotor thrust and torque values. Altogether, this causes complex pulsations of rotor thrust and torque, which will be presented and analyzed below. Figures 17 and 18 show the calculated dependences of thrust c_T and torque c_Q coefficients of 3-bladed and scissors rotors on number of revolutions n for $V_y = 10, 12, 14$ and 18 m/s.

Figures 17(a), 17(c), 17(e) and 17(j) show the dependences of $c_T = f(n)$ for a 3-bladed rotor, including: the dependences of the time-averaged thrust (bold dotted line in green), the dependences of the instantaneous thrust (shown in light green) and the dependences of the averaged thrust (shown in green bold line). Figures 17(b), 17(d), 17(f) and 17(k) show similar dependencies for the total thrust of the upper and lower couple of blades of scissors rotor, here $c_T = c_{TU} + c_{TL}$. The curves for the scissors rotor, in contrast to the curves for the 3-bladed rotor, are represented in blue colors on the diagrams, as in the entire article. In addition, for the scissors rotor, the dependences of the averaged values of the thrust of the upper and lower couple of blades are also plotted separately.

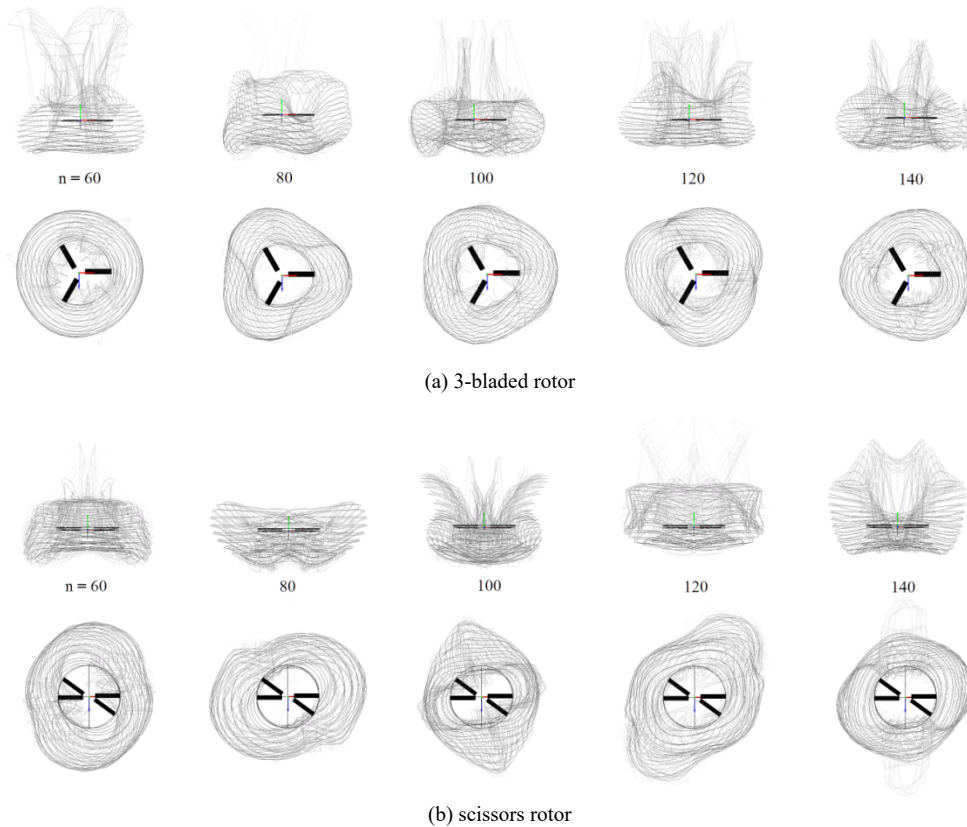
Diagrams on Figs. 17 illustrate the relationship between features of the flow around the rotor in the VRS modes with the observed pulsations of aerodynamic forces. Instantaneous thrust pulsations have a frequency of about 40 Hz (2-3 repetitions per one rotor turn). In Fig. 17 instantaneous thrust curves merge into a solid area. As it is mentioned above, they are caused by the rotation of the rotor in an asymmetric velocity field relative to the axis of rotation of the rotor. Thus, they are associated with the axial asymmetry of the vortex wake.

In turn, the instability of the rotor flow over time, reflected in a change in the vortex wake shape and position relative to the rotor (Figs. 15 and 17) causes unstable pulsations of averaged thrust and torque. These pulsations with a period of few rotor turns are shown in Figs. 17 by the curves of averaged thrust. The rotor thrust pulsations noted above in the VRS modes are well known and observed in experiments [3], [4], [8], [11].

From Figs. 17 it can be noted that the pulsations of the scissors rotor average thrust at $V_y = 12$ and 14 m/s are significantly less than those of 3-bladed rotor. This was shown earlier in Figure 13. Figures 18(a), 18(c), 18(e) and 18(j) show the dependencies of torque coefficient $c_Q = f(n)$ for 3-bladed rotor, and Fig. 18(b), 18(d), 18(f) and 18(k) – for scissors rotor. Here, as in Figs. 18, the dependences of the instantaneous, averaged and time-averaged torque coefficients on the number of revolutions of the rotor n are shown. The time-averaged coefficient of rotor thrust for operating modes shown in Figs. 18 is constant and equal to $c_T = 0.02$.



Figs. 15. Visualization of the flow structure around the rotors $c_T = 0.02 = \text{const}$



Figs. 16. Visualizations of the vortex wake shapes in the VRS mode ($V_y = 12$ m/s) for different number of revolutions n

In this case, the torque coefficient for various V_y velocities will be different (Fig. 12). All diagrams also show the values of the c_Q coefficient for the hovering mode (for $c_T = 0.02 = \text{const}$). In the VRS mode, an increase in the time-averaged value of the c_Q coefficient is observed comparing to the hovering mode. Scissors rotor has a 21% increase in torque at $V_y = 12$ m/s (Fig. 18(d)). 3-bladed rotor has 26% increase (Fig. 18(c)). From the dependences of the averaged coefficient c_Q , shown in Figs. 18 for $V_y = 12$ and 14 m/s, it can be seen that the scissors rotor has significantly lower pulsations amplitude than 3-bladed rotor.

Figure 19 shows a diagram of the distribution of the time-averaged values of the thrust coefficients between the upper and lower couples of blades of scissors rotor: $c_{TU} = f(V_y)$ and $c_{TL} = f(V_y)$.

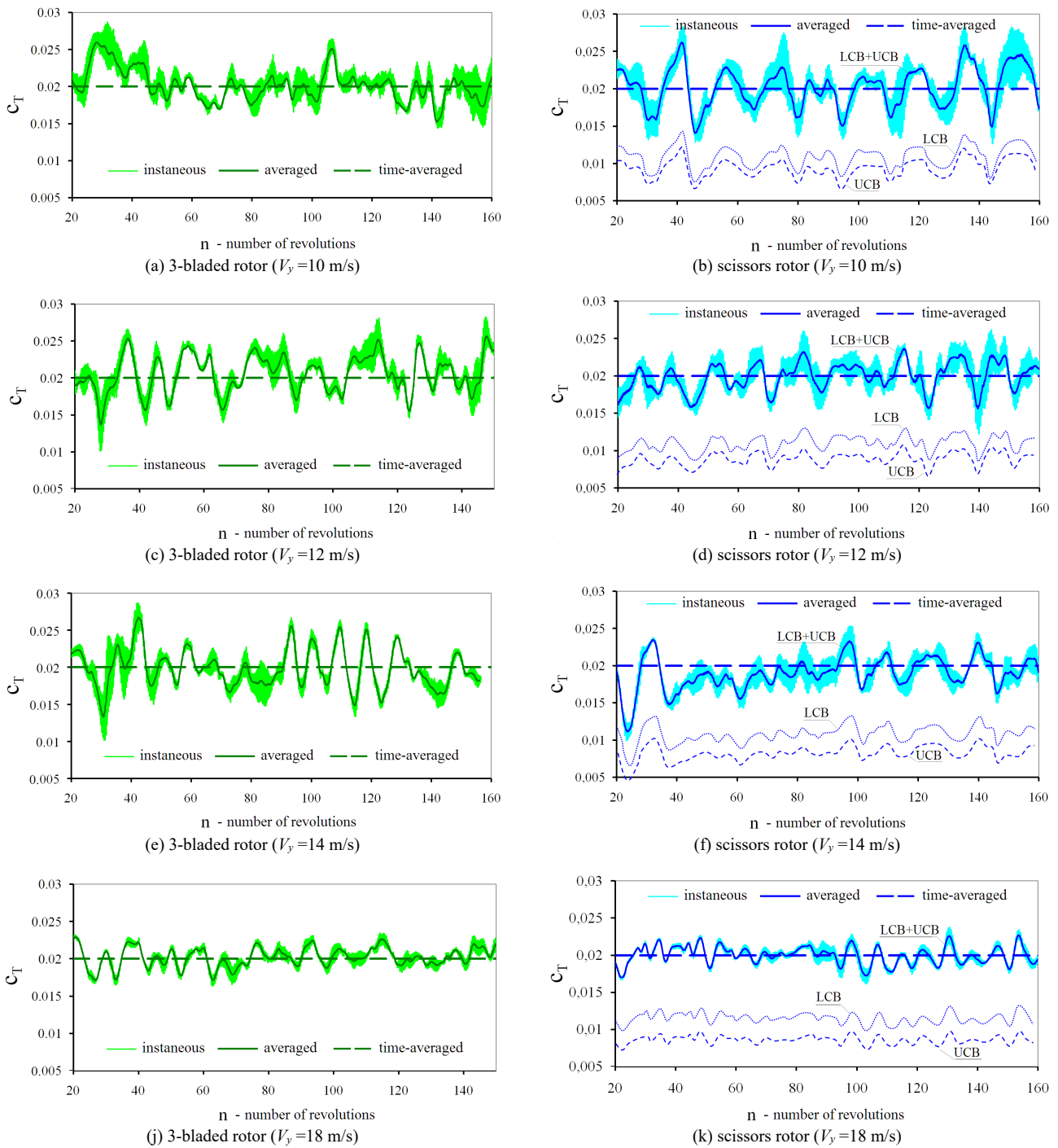
The dependences of thrust coefficients $c_{TU} = f(n)$ and $c_{TL} = f(n)$ for $V_y = 10, 12, 14$ and 18 m/s had been presented above in Figs. 17. It can be seen that at the entire axial flow velocity range $V_y = -15 - 25$ m/s the thrust of the lower couple of blades is greater than the thrust of the upper couple of blades (provided that their blade pitch angles are equal $\theta_U = \theta_L$).

At negative ($\alpha_R = -90^\circ$, $V_y = -15 - 0$ m/s) angles of attack $c_{TL} / c_{TU} \approx 1.17 - 1.14$, at hover $c_{TL} / c_{TU} \approx 1.13$, and at positive ($\alpha_R = 90^\circ$, $V_y = 0 - 25$ m/s) angles of attack $c_{TL} / c_{TU} \approx 1.15 - 1.5$. The present hypothesis about the relationship between the obtained thrust and torque pulsations and features of the flow around the studied rotors in the VRS modes requires additional analysis,

which is given below. Figures 20 show the results of the analysis of the thrust pulsations of a 3-bladed rotor observed in the VRS modes. There have been used fragments of $c_T = f(n)$ diagram from Fig. 17(c) for $n = 105-125$. With the scale used, periodic pulsations of instantaneous thrust (light green curve) with a high frequency are clearly visible. The figure also shows the dependence of the averaged thrust (dark green curve), which varies over time with a large amplitude and period according to a complex law.

Figures 16 have previously showed that the shape of the vortex wake and its position relative to the rotor's rotational plane in the VRS modes are significantly changing over time.

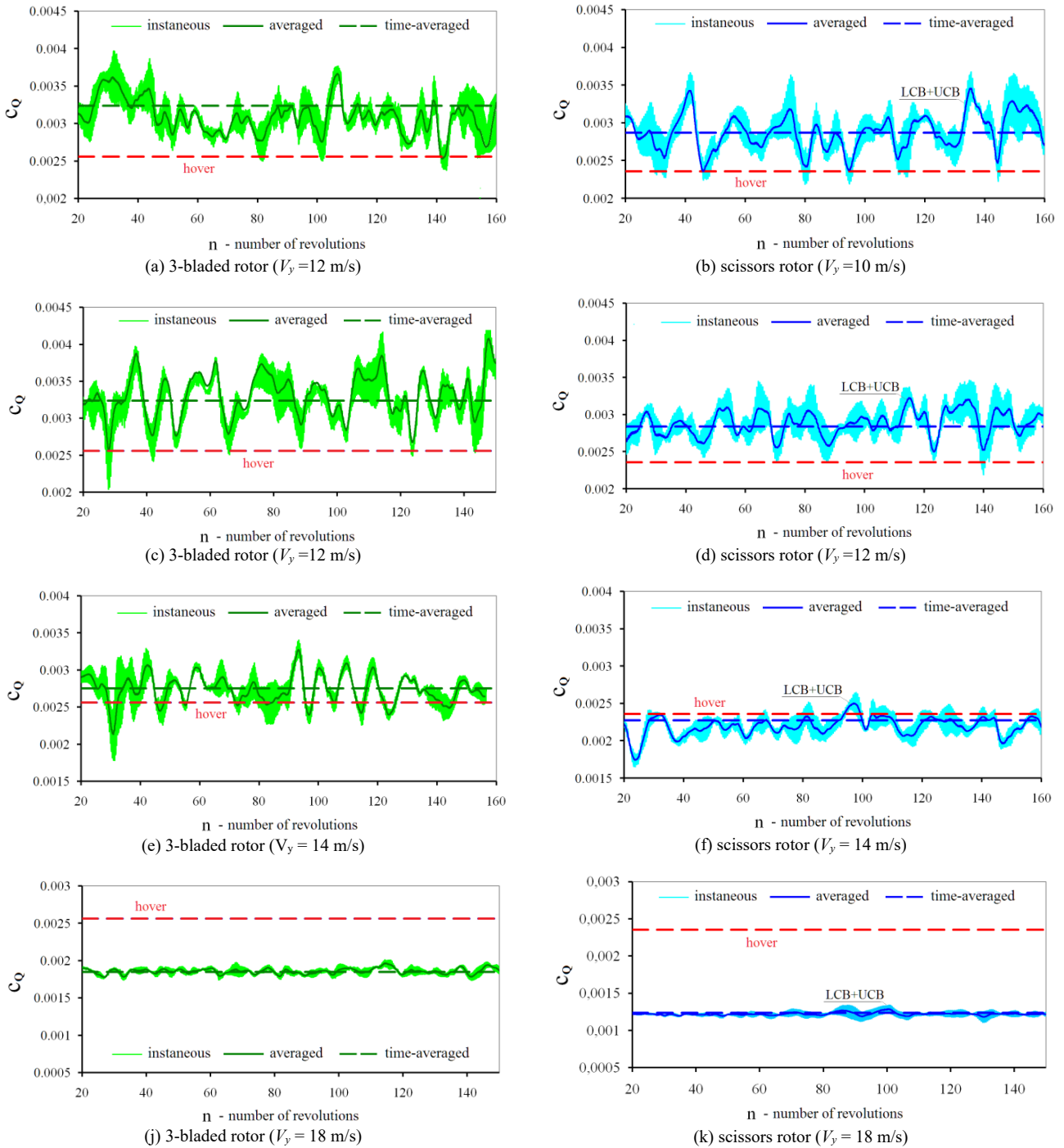
Figs. 20 also include three images of the rotor flow for different time points. Point A corresponds to the maximum value of the average thrust ($c_T \approx 0.025$), point B corresponds to the average value ($c_T \approx 0.02$), point C corresponds to the minimum value ($c_T \approx 0.015$). It can be seen that for all three cases, the position of the axis of the "vortex ring" ("air body") relative to the rotor's rotational plane differs significantly. Such an effect, typical for the unsteady flow around the rotor in the VRS modes, is the reason for the complex non-periodic pulsations of the average thrust over time noted in Figs. 18. For the analysis of instantaneous thrust pulsations, Fig. 20(b) shows a fragment of the dependence $c_T = f(n)$ from Fig. 20(a) for one turn of the rotor ($n = 111 - 112$). Instantaneous thrust pulsations have a frequency of about 60 Hz (3 repetitions per 1 rotor revolution).



Figs. 17. Dependences of thrust coefficients vs. rotor revolutions number n of scissors and 3-bladed rotors for various V_y values

The points D, E and F corresponding to the maximum, average and minimum values of the instantaneous thrust of the rotor are marked on the curve $c_T = f(n)$. For these points the diagrams of induced velocity V_y in the rotors rotational plane are also shown here. Comparison of the position of the blades with the current instantaneous thrust value confirms that its periodic pulsations in the VRS modes are caused by the rotation of the blades in an asymmetric induced velocities' field. Figures 21 show the results of the analysis of thrust pulsations for scissors rotor. Figure 21(a) shows a fragment of the diagram from Fig. 17(d) for $n = 125-150$.

Three flow pictures for different values of the averaged thrust are shown: point A corresponds to the maximum thrust value ($c_T \approx 0.023$), point B corresponds to the average thrust value ($c_T \approx 0.02$), and point C corresponds to the minimum thrust value ($c_T \approx 0.0155$). As in the case of a 3-bladed rotor, the position of the axis of the "vortex ring" (visualized by an "air body" with circulating flow inside) relative to the rotors rotational plane differs significantly for the considered points. Figure 21(b) shows a fragment of the dependence of $c_T = f(n)$ from Fig. 21(a) for $n = 131 - 132$.



Figs. 18. Dependences of torque coefficients vs. rotor revolutions number value n of scissors and 3-bladed rotors for various V_y values

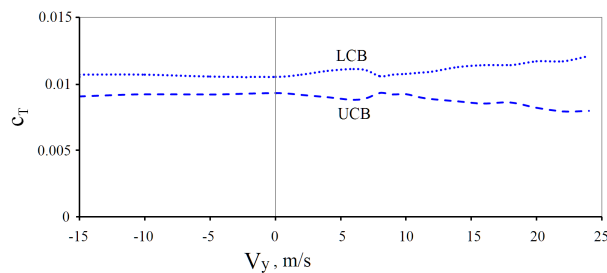
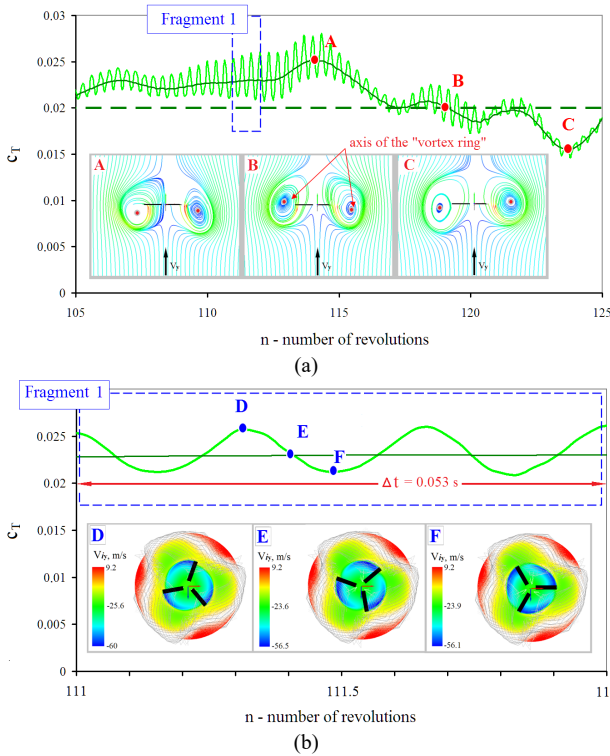
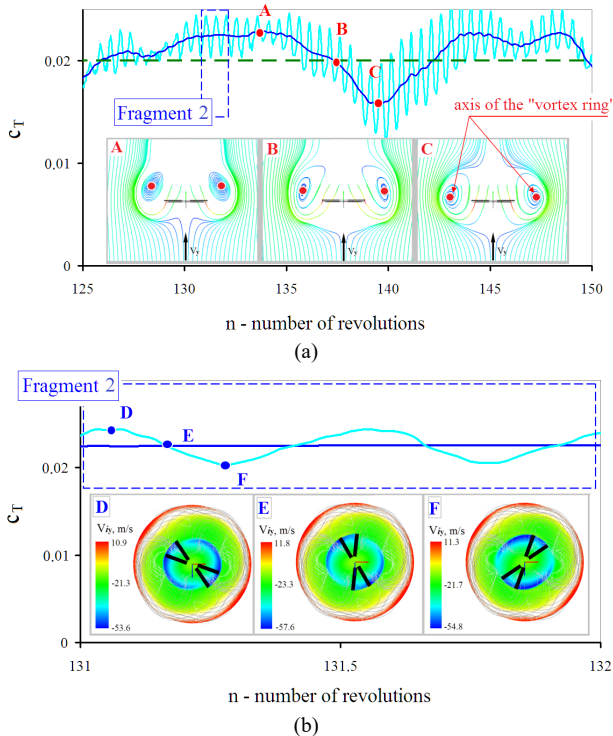


Fig. 19. Distribution of the time-averaged thrust coefficient between the upper and lower couple of blades of scissors rotor on the various axial velocity V_y ($\theta_U = \theta_L$, $c_T = 0.02 = \text{const}$)



Figs. 20. Analysis of averaged and instantaneous thrust pulsation of 3-bladed rotor in the VRS mode (fragment of the Fig. 18(c), $V_y = 12$ m/s, $n = 105 - 125$ and $n = 111 - 112$)



Figs. 21. Analysis of averaged and instantaneous thrust pulsation of scissors rotor in the VRS mode (fragment of Fig. 18(d), $V_y = 12$ m/s, $n = 125 - 150$ and $n = 131 - 132$)

Here the pulsations of instantaneous thrust have a frequency of about 40 Hz (2 repetitions per 1 revolution). This is due to the specifics of the scissors rotor

geometry, which has 4 blade with "scissors" angle of 36° .

The points D, E and F are marked, corresponding to the maximum, average and minimum values of the instantaneous thrust. For these points, diagrams of the induced velocity V_y are given. It can be seen that periodic pulsations of the instantaneous thrust value are associated with the rotation of the scissors rotor in an asymmetric induced velocities' field.

IV. Conclusion

Based on the original free wake model, comparative study of axial flow modes aerodynamics of 3-bladed and scissors tail rotors used on Mi-8/17 helicopter series have been performed. The wide axial velocity range $V_y = -15 - 25$ m/s and two various approaches: fixed rotor thrust ($c_T = 0.02$) and fixed rotor blade pitch angle (corresponding to $c_T = 0.02$ in hover) have been considered. For the hovering mode it has been shown that scissors rotor has an advantage of up to 10% in the Figure of Merit value in comparison with 3-bladed rotor. For the axial flow modes it was shown that the thrust of the LCB exceeds the thrust of the UCB by an amount from 13% to 50% at equal LCB/UCB blade pitch angles. For the axial flow modes with positive angles of attack of a rotor, the VRS modes area have been investigated. By criterion of rotor thrust reducing at a fixed blade pitch angle, the VRS area of scissors and 3-bladed rotor coincides and is in the range of $V_y = 8.5 - 15.7$ m/s. By criterion of growth of rotor torque relative to the torque in hover ($c_Q > c_{Qh}$) at a fixed thrust ($c_T = 0.02 = \text{const}$), the VRS area for scissors rotor is in the range of $V_y = 7.3 - 14$ m/s, and for 3-bladed rotor is in the range of $V_y = 7.7 - 15$ m/s. It has been found that for the equal thrust force value scissors rotor has a 4% lower increase in the required power in the VRS modes than 3-bladed rotor. The rotor thrust and torque pulsations in the VRS modes have been analyzed.

It was established that the high frequency instantaneous thrust pulsations depend on the rotor geometry and are associated with the rotation of the blades in an asymmetric induced velocity field. It was shown that complex pulsations of averaged thrust with the large amplitude and period are associated with changes in time in the structure and position in space of the rotors vortex wake. A comparative analysis of the averaged thrust and torque pulsations in the VRS modes showed that scissors rotor in the range of $V_y = 12 - 16$ m/s (most intense VRS modes) has 1.5 - 2 times less amplitude of pulsations than that of a 3-bladed rotor. The results of the comparative studies indicate a greater efficiency of the improved aerodynamic design of the scissors tail rotor both when hovering and when falling into the VRS modes compared to the 3-bladed rotor, which is important for a single-rotor helicopter.

References

- [1] J. Drees, W. P. Hendl, The Field of Flow through a Helicopter Rotor Obtained from Wind Tunnel Smoke Tests. *Journal of*

- Aircraft Engineering*, 1951, 23(226) 107.
- [2] J. Castles, R. B. Gray, *Empirical Relation between Induced Velocity, Trust, and Rate of Descent of a Helicopter Rotors as Determined by Wind-Tunnel Tests on Four Model Rotors*, NACA TN-2474, (1951).
https://archive.org/details/nasa_techdoc_19930083181
- [3] P. F. Yaggy, K. W. Mort, *Wind-Tunnel Tests of Two VTOL Propellers in Descent*, NASA TN D-1766, (1963).
https://archive.org/details/nasa_techdoc_19630003345/mode/2up
- [4] K. Washizu et al, Experiments on a Model Helicopter Rotor Operating in the Vortex Ring State, *J Aircr* 1966;3:225–30.
 doi: <https://doi.org/10.2514/3.43729>
- [5] R. W. Empey, R. A. Ormiston, Tail-Rotor Thrust on a 5.5-Foot Helicopter Model in Ground Effect. *The 30th annual forum of the American helicopter society*, (1974).
- [6] H. Xin, Z. Gao, A Prediction of the Helicopter Vortex-ring State Boundary, *Journal of Experiments in Fluid Mechanics*, 1996;01:14-19.
- [7] P. Brinson, T. Ellenrieder, Experimental Investigation of the Vortex Ring Condition. *The 24th European Rotorcraft Forum*, (1998).
- [8] M. D. Betzina, Tiltrotor Descent Aerodynamics: A Small-Scale Experimental Investigation of Vortex Ring State. *The 57rd annual forum of the American Helicopter Society*, (2001).
- [9] R. Green et al, The flow field around a rotor in axial descent, *Journal of Fluid Mechanics*, Vol. 534, 2005, pp. 237-261.2005.
 doi: 10.1017/S00222112005004155
- [10] F. X. Caradonna, Performance measurement and wake characteristics of a model rotor in axial flight, *J Am Helicopter Soc* 44(2):101-108.
- [11] J. Stack et al, Flow Visualizations and Extended Thrust Time Histories of Rotor Vortex Wakes in Descent, *J Am Helicopter Soc*, 2005;50:279–88.
 doi: <https://doi.org/10.4050/1.3092864>
- [12] V. V. Efimov, K. O., Chernigin, Vortex ring state as a cause of a single-rotor helicopter unanticipated yaw, *AS*, 2022.
 doi: <https://doi.org/10.1007/s42401-021-00128-4>
- [13] J. G. Leishman et al, Free-Vortex Wake Predictions of the Vortex Ring State for Single Rotor and Multi-Rotor Configurations. *The 58th annual forum of the American Helicopter Society*, (2002).
- [14] R. Celi, M. Ribera, Time Marching Simulation Modeling in Axial Descending through the Vortex Ring State. *The 63rd annual forum of the American Helicopter Society*, (2007).
- [15] J. Bailly, A Qualitative Analysis of Vortex Ring State Entry Using a Fully Time Marching Unsteady Wake Model. *The 36th European Rotorcraft Forum*, (2010).
- [16] V. M. Shcheglova, Non-Stationary Rotor Flow in the Steep Descent State and the VRS, *Uchenye Zapiski TsAGI*, 2012; 43(3):51–8 (in Russian).
- [17] W. Stalewski, K. Surmacz, Investigations of the vortex ring state on a helicopter main rotor using the URANS solver, *Aircraft Engineering and aerospace Technology*, 2020, Vol. 92 No. 9, pp. 1327-1337.
 doi: <https://doi.org/10.1108/AEAT-12-2019-026>
- [18] N. Mohd, G. Barakos, Performance and Wake Analysis of Rotors in Axial Flight Using Computational Fluid Dynamics, *J Aerosp Technol Manag*, 2017;9:193–202.
 doi: <http://dx.doi.org/10.5028/jatm.v9i2.623>
- [19] M. P. Kinzel et al, An investigation of the behavior of a coaxial rotor in descent and ground effect. *The AIAA Scitech 2019 Forum*, (2019).
- [20] J. McQuaid et al, Early Onset Prediction for Rotors in Vortex Ring State, *Journal of Aerospace Engineering*, 2020, 33. 04020081.
 doi: [https://doi.org/10.1061/\(ASCE\)AS.1943-525.0001194](https://doi.org/10.1061/(ASCE)AS.1943-525.0001194)
- [21] K. Ryan et al, Propeller and vortex ring state for floating offshore wind turbines during surge, *Renewable Energy*, 2020, Volume 155, 645-657.
 doi: <https://doi.org/10.1016/j.renene.2020.03.105>
- [22] J. Dong, A. Vire, Comparative analysis of different criteria for the prediction of vortex ring state of floating offshore wind turbines. *Renewable Energy*, 2021, 163. 882-909.
 doi: 10.1016/j.renene.2020.08.027
- [23] Yu. M. Ignatkin et al, A Nonlinear Blade Vortex Propeller Theory and Its Applications to Estimate Aerodynamic Characteristics for Helicopter Main Rotor and Anti-Torque Rotor, *Vestnik MAI*, Vol. 16, No. 5, 2009, pp. 24-31. (In Russian).
<http://vestnikmai.ru/eng/publications.php?ID=12351&eng=Y>
- [24] P. Makeev et al., Numerical study of the main rotor steep descent modes in the vortex ring state area, *J. Phys.: Conf. Ser.* 2021, 1925 012004.
 doi: 10.1088/1742-6596/1925/1/012004
- [25] P. V. Makeev et al, Numerical investigation of full scale coaxial main rotor aerodynamics in hover and vertical descent, *Chinese Journal of Aeronautics*, Volume 34, Issue 5, 2021, pp. 666-683.
 doi: <https://doi.org/10.1016/j.cja.2020.12.011>
- [26] M. G. Rozhdestvensky, Scissors rotor concept-new results obtained. *The 52th annual forum of the American Helicopter Society*, (1996).
- [27] G. H. Xu, An experimental and analytical investigation of scissors rotor aerodynamics in hover. *The 60th annual forum of the American Helicopter Society*, 2004, vol. 1, pp. 54-62.
- [28] G. H. Xu, Study on the Induced Velocity and Noise Characteristics of a Scissors Rotor. *J Aircraft*, 2007, 44. 806-811.
 doi: 10.2514/1.24460
- [29] Z. Zhu et al, Studies on vortex interaction mechanism and aerodynamic characteristic of scissors tail rotor. *Chinese Journal of Theoretical and Applied Mechanics*, Vol. 48(4), 2016, pp. 886-896.
 doi: 10.6052/0459-1879-15-338
- [30] D. Uehara et al, Hover Performance of Corotating and Counterrotating Coaxial Rotors, *Journal of the American Helicopter Society*. Vol. 38, No. 2, 2019, pp. 1-8.
 doi: 10.4050/JAHS.65.012006.
- [31] M. Bhagwat, Co-rotating and Counter-rotating Coaxial Rotor Performance, *AHS Aeromechanics Design for Transformative Vertical Flight*, (2018).
- [32] S. Platzer et al, Investigation of the Flow Fields of Coaxial Stacked and Counter-Rotating Rotors Using PIV Measurements and URANS Simulations. *Vertical Flight Society's 77th Annual Forum & Technology Display At: Virtual*, (2021).
- [33] C. Coleman, *A Survey of Theoretical and Experimental Coaxial Rotor Aerodynamic Research*. Report №.: NASA TP-3675, (1997).
- [34] H. W. Kim, R. E. Brown, A Comparison of Coaxial and Conventional Rotor Performance, *Journal of the American Helicopter Society*, Vol. 55, No. 1, 2010.
 doi: <https://doi.org/10.4050/JAHS.55.012004>

Authors' information

¹Moscow Aviation Institute (National Research University), Moscow, Russia.

²JSC Helicopters Mil & Kamov, Moscow region, Russia.



Pavel V. Makeev is Ph.D of Engineering Sciences, Associate professor at the Helicopter Design Department of Moscow Aviation Institute (National Research University). Research interests include computational fluid dynamics and helicopter aerodynamics.
 E-mail: MakeevPV@mai.ru



Yuri M. Ignatkin is Ph.D of Engineering Sciences, Associate professor at the Helicopter Design Department of the Moscow Aviation Institute (National Research University). Research interests include experimental aerodynamics, computational fluid dynamics and helicopter aerodynamics.
 E-mail: IgnatkinYM@mai.ru



Alexander. I. Shomov is Ph.D of Engineering Sciences, Associate professor at the Helicopter Design Department of Moscow Aviation Institute (National Research University). Research interests include aerodynamics and helicopter design.
E-mail: Shomov_Aleksandr@mail.ru



Valery A. Ivchin is Ph.D of Engineering Sciences, Deputy chief designer of the JSC Helicopters Mil & Kamov, Moscow region, Russia. Research interests include helicopter aerodynamics, dynamics and helicopter design
E-mail: valivchin@mail.ru